Transactions, **SMiRT-26**
Berlin/Potsdam, Germany, July 10-15, 2022
Division V

EFFECTS OF NEAR-FAULT GROUND MOTIONS ON NUCLEAR POWER PLANT CONTAINMENT STRUCTURES

Kurtuluş Soyluk[1], Hamid Sadegh-Azar[2], Dersu Yılmaz[3]

[1] Gazi University, Faculty of Engineering, Department of Civil Engineering, Ankara, TURKEY (ksoyluk@gazi.edu.tr)
[2] TU Kaiserslautern, Institute of Structural Analysis and Dynamics, Department of Civil Engineering, Kaiserslautern, GERMANY
[3] Pohlcon GmbH, 12057 Berlin, GERMANY

ABSTRACT

In this study, it is intended to perform nonlinear time-history analyses of nuclear power plant structures (NPP) under near-fault earthquakes showing directivity pulse and fling-step characteristics. The structural responses obtained for the near-fault earthquakes are compared with those of the results obtained from the far-fault ground motions. Because it is aimed to determine specifically the pulse type characteristics of near-fault ground motions on NPPs, two different normalization strategies are used to compare the results in a consistent manner. The containment building considered in this study has a cylindrical wall connected with a spherical dome. Depending on the obtained results it can be outlined that especially the directivity-pulse characteristics of near fault ground motions have noticeable effects on the responses of the considered NPP containment building.

INTRODUCTION

Near-fault ground motions are different from ordinary ground motions in that they often contain strong coherent dynamic long period pulses and permanent ground displacements. The dynamic motions are dominated by a long period pulse of motion that occurs on the horizontal component perpendicular to the strike of the fault, caused by rupture directivity (directivity-pulse) effects. The static ground displacements in near-fault ground motions are caused by the relative movement of the two sides of the fault on which the earthquake occurs (fling-step effect). These displacements are discontinuous across a fault having surface rupture and can subject a structural system crossing a fault to significant differential displacements. The static ground displacements occur at about the same time as the large dynamic motions, indicating that the static and dynamic displacements need to be treated as coincident loads. These dynamic motions and static ground displacements are defined by “directivity-pulse” and “fling step” effects (Somerville, 2002). Although some codes take into account the near-fault effects through some amplification factors, further studies should be conducted so that this effect can be included in codes in a more realistic way. According to IAEA 2009, “most of near field earthquakes of small magnitude (i.e. $M \leq 5.5$) have high frequency content and produce high peak ground acceleration levels, but they do not generate significant damage to structures and mechanical equipment. However, if the high frequency content produced by such near field earthquakes is transmitted to the structures, it may cause operability problems with certain types of equipment.” On the other hand, the location of recent Niigata Chuetsu-Oki earthquake of magnitude 6.6 was very close to the nuclear power plant site Kashiwazaki Kariwa and the measured ground acceleration was much larger (0.69g) than those of the safety earthquake for the plant site (EnBW, 2008). Therefore, the possible effect of near-fault earthquakes on NPP structures should be carefully investigated.

Although many studies have been performed to determine the seismic responses of structural systems under near fault ground motions so far, studies investigating the seismic responses of NPPs under near-fault ground motions are rather limited (Galal and Ghobarah, 2006; Choi et al., 2010; Longjun et al., 2010; Labbe and Altınyollar, 2011; Mena JAA, 2016; Jin and Gong, 2020). In this study, it is intended to perform nonlinear time-history analyses of NPPs specifically for near-fault ground motions showing directivity pulse and fling-step characteristics. Then, the structural responses are compared with those of the results obtained from the far-fault ground motions.

NUCLEAR POWER PLANT (NPP) CONTAINMENT BUILDING GEOMETRY

The nuclear power plant containment building that is considered in this study is a typical containment building, which has a cylindrical wall connected with a spherical dome. The dome is monolithic to that of the cylinder with equivalent thickness. While the radius of the cylinder and the hemispherical shell are 22 m, the height of the cylinder is 44 m (Lu X et al., 2015). The geometry of the containment building is shown in Figure 1. The wall of the containment building is considered as 1 m thick concrete doubly reinforced with 40 mm diameter bars placed 80 mm along the meridional and circumferential directions at inner and outer faces of the dome and cylinder. The concrete cover is considered as 100 mm at both faces (Sadique MR et al., 2013). Fixed base conditions are assumed for the containment building.

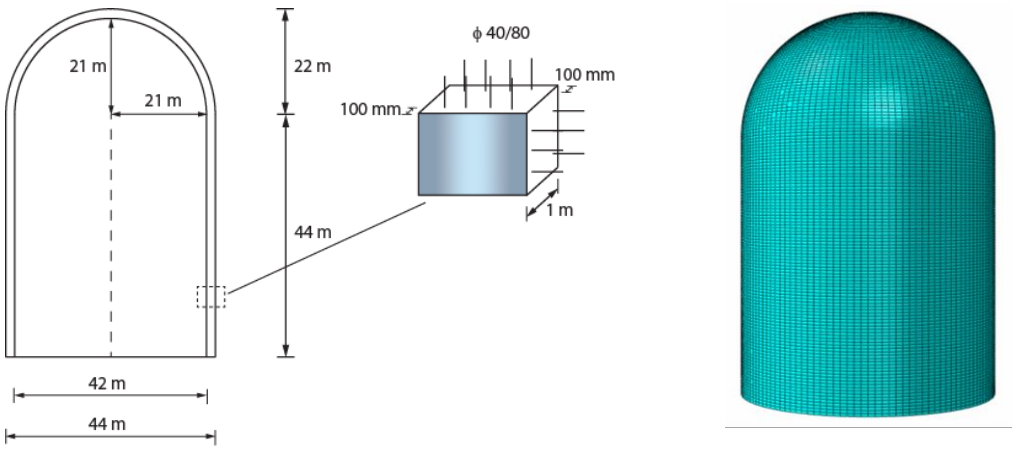

Figure 1. Cross-sectional view, reinforcement detailing and FE model of the containment building

The concrete damaged plasticity (CDP) model provided in ABAQUS for the analysis of concrete material is used as the constitutive model. B50 grade concrete is used for the containment building and the parameters of the concrete damage plasticity model, including a damage parameter, strain hardening/softening rules, and certain other elements, are obtained from Esfahani MH et al. (2017). Mechanical properties of the concrete used in this study are given in Table 1. The remaining parameters related to the concrete damage plasticity model can be obtained from Esfahani MH et al. (2017). For the containment building SA738 Grade B steel, which is assumed to have uniaxial properties in the direction of the bars, is used. Considering the fact that the reinforcing steel shows a strain hardening behavior under earthquake motions, the bilinear kinematic hardening model available in ABAQUS is used as the constitutive model for the steel material. Mechanical properties of the reinforcing steel used in this study is given in Table 2. FE model of the containment structure is meshed using layered shell element option in ABAQUS. The rebar layers are defined at the inner and outer faces of the 1 m thick concrete layer of the dome and cylinder along the meridional and circumferential directions. Figure 1 shows the 3D finite element model of the containment structure. The global mesh size is selected as 0.5 m x 0.5 m and linear quadrilateral shell elements of type S4R are used in the FE model.

Table 1. Material properties of concrete (Esfahani MH et al., 20116)

Density (kg/m^3)	Young's Modulus (GPa)	Poisson's Ratio	Compressive Stress (MPa)
2400	33.4	0.2	50

Table 2. Material properties of reinforcing steel (Ma et al., 2016)

Density (kg/m^3)	Young's Modulus (GPa)	Poisson's Ratio	Yield Stress (MPa)	Tensile Stress (MPa)
7850	210	0.3	503.06	603.43

NEAR-FAULT GROUND MOTIONS

Near-fault ground motion components of Chi-Chi earthquake, with a moment magnitude M_w=7.62, showing forward-directivity and fling-step characteristics as well as far-fault ground motions obtained from PEER Ground Motion Database are used in this study (Table 3).

Table 3. Characteristics of near-fault and far-fault ground motion components of Chi-Chi earthquake

Component	Fault Distance d (km)	PGA (g)	PGV (cm/s)	PGV/PGA (sec)	Fling Step (cm)
Near Fault Recordings (Forward Directivity)					
TCU052-EW	0.66	0.357	151.10	0.431	
TCU053-EW	5.95	0.229	39.579	0.176	
TCU068-EW	0.32	0.512	249.38	0.501	
TCU075-EW	0.89	0.331	109.46	0.337	
TCU082-EW	5.16	0.225	54.895	0.249	
TCU101-EW	2.11	0.212	76.770	0.369	
TCU103-EW	6.08	0.129	70.219	0.555	
Near Fault Recordings (Fling-Step)					
TCU068-NS	0.32	0.378	293.58	0.792	594.984
TCU074-NS	13.46	0.388	48.169	0.127	92.5870
TCU089-NS	9.00	0.243	30.728	0.129	63.7520
TCU102-NS	1.49	0.173	65.500	0.386	126.397
TCU129-NS	1.83	0.629	50.993	0.083	96.0570
Far Fault Recordings					
CHY014-NS	34.18	0.260	22.95	0.090	
CHY052-NS	39.02	0.154	14.69	0.097	
CHY088-NS	37.48	0.211	20.74	0.099	
HWA032-NS	47.31	0.110	8.170	0.076	
HWA034-NS	44.32	0.142	10.98	0.080	
HWA037-EW	46.20	0.110	12.78	0.118	
ILA067-EW	38.82	0.199	11.81	0.060	

As can be observed, 7 near-fault ground motions showing forward-directivity effect, 5 near-fault ground motions showing fling-step effect and 7 far-fault ground motions are used in this study. While the near-fault ground motions are recorded mostly within 5 km from the fault, the far-fault ground motions are recorded within 50 km. For the ground motion components showing forward-directivity and fling-step

characteristics, the ratio of PGV/PGA is calculated as larger than 0.1, indicating the near-fault effect of these ground motion components. As can be noticed, the selected ground motions have peak accelerations from 0.11g to 0.629g. To be able to investigate the pulse type characteristics of the near-fault ground motions, first all the selected ground motion components are scaled to the design earthquake level of 0.3g for a fair comparison. Considering the fact that each selected ground motion has a different acceleration spectrum at the fundamental period of the NPP after the normalization, it is also intended to scale the ground motions to have the same acceleration spectrum at the fundamental period. Hence, the acceleration spectrum of each ground motion component is normalized to $Sa(T_1)$=0.6g as the average acceleration spectrum of the considered ground motions. Alavi and Krawinkler (2004) and Kalkan and Kunnath (2006) had also scaled the ground motions to match with the design spectrum for the comparison of results from different ground motion sets in a consistent manner.

Acceleration, velocity and displacement time-history plots of the selected ground motions belonging to each group of ground motions showing forward-directivity and fling-step characteristics as well as far-fault ground motion are given in Figures 2-4. Remarkable pulse characteristics can be noticed in the velocity-time history graphs of the near-fault ground motions.

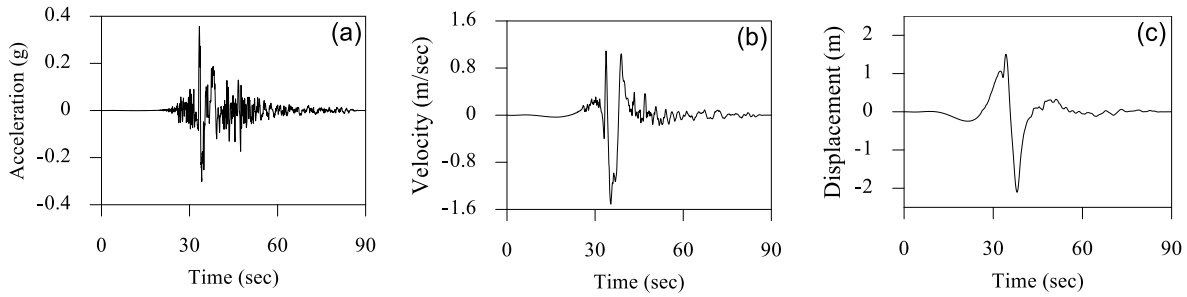

Figure 2. a) Acceleration, b) Velocity, c) Displacement; time histories of TCU052EW record

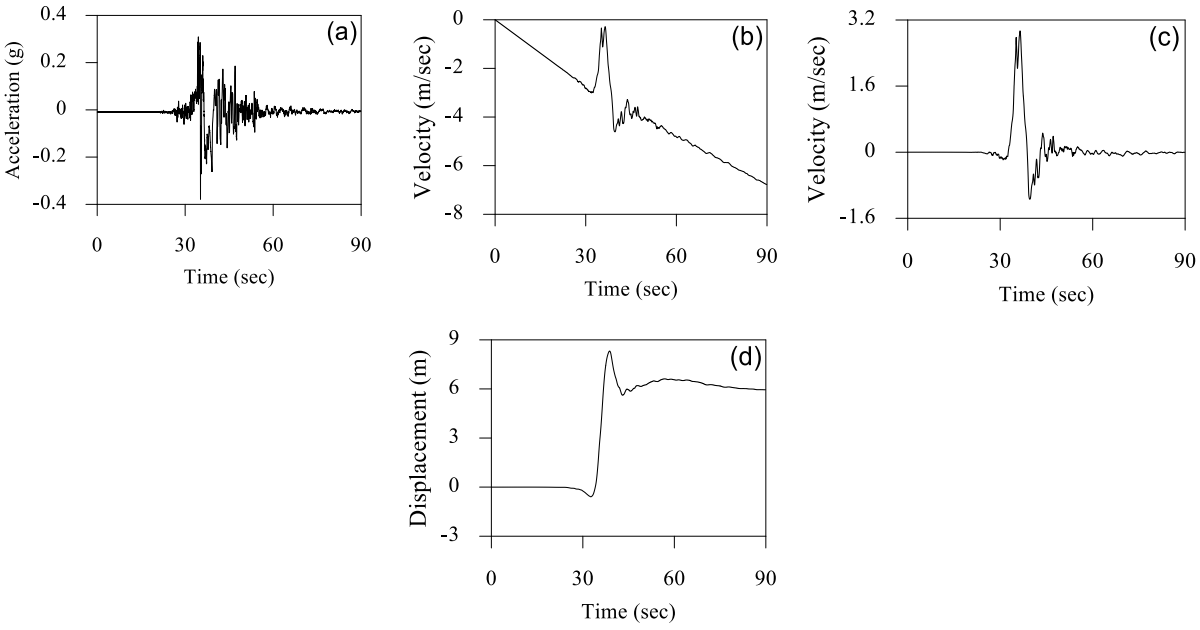

Figure 3. a) Raw acceleration, b) Integrated velocity, c) Baseline corrected velocity, d) Integrated displacement; time histories of TCU068NS record

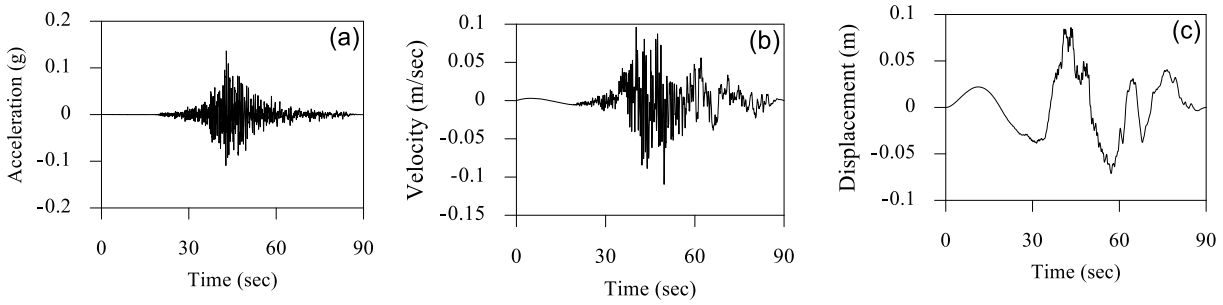

Figure 4. a) Acceleration, b) Velocity, c) Displacement; time histories of HWA034NS record

The displacement time histories obtained through the PEER Strong Motion Database do not show static displacements due to the applied standard data processing procedures (Darragh et al, 2004). Therefore, in order to be able to investigate the fling-step effect, raw recordings are required so that displacement-time history recordings showing static displacements can be obtained. In this paper, integrations are performed through the raw acceleration-time histories of TCU068-NS, TCU074-NS, TCU089-NS, TCU102NS and TCU129NS recordings obtained from Boore (2001) to get the velocity-time and displacement-time history plots (Figure 3). But due to the technical reasons related to the sensitivity of the instruments and secondary vibrations in the environment, the velocity-time history plots obtained from the integration of the recordings do not come to rest at the end of the motion (Figure 3b). Considering the fact that the velocity is not zero at the end of the motion, it becomes necessary to apply a correction to the recording. Therefore, a baseline correction procedure is applied to the velocity-time history plot which is determined from the integration of the acceleration-time history graph so that velocity-time history plot has a zero ending (Figure 3c). Then, this velocity-time history plot is integrated once more to get the displacement-time history with permanent ground displacements (Figure 3d). As a result of the fling-step effect, 5.95 m static ground displacement is observed at the end of the TCU068-NS recording. In this study OriginPro (2021) software is used for the integration and baseline correction of these records.

Considering the fact that the selected far-fault ground motion components of Chi-Chi earthquake are between 35-50 km from the fault, they are considered as far fault ground motions. On the other hand, it is also possible to observe that the displacement-time history and the velocity-time history plots of these records do not show any fling-step and directivity pulse characteristics (Figure 4). As expected, the ratio of PGV/PGA is usually smaller than 0.1.

Normalized acceleration response spectrum of each ground motion component belonging to a group of forward-directivity records, fling-step records and far-field records are plotted in Figures 5-7, and an average acceleration response spectrum (red lines) is obtained for each group of ground motion. Then, these mean response spectra are compared with the design spectrum of UBC 97 for a damping ratio of 5% (Figure 8).

The design spectrum is constructed for soil profile type S_C, seismic zone factor of 4, seismic source type A and fault distance of 5 km. The design spectrum parameters are selected to consider also the near-fault effects through the near-source amplification factors of Na and Nv given in UBC 97. As expected, near-fault ground motions with forward-directivity and fling-step effects have specific characteristics if compared with the far-fault ground motions. From the response spectra it can be noticed that near-fault ground motions with forward-directivity and fling-step characteristics exceed the design spectrum mainly for long periods above 1.0 sec indicating the presence of near-fault effects. Hence, this acceleration response spectrum reveals that near-fault ground motions have the potential to cause damage mostly on structural systems having larger periods. On the other hand, near-fault ground motions with forward-directivity

characteristics and far-fault ground motions exceed the design spectrum even for some short periods. This observation necessities the consideration of near-fault effects even for stiff structures, like NPPs.

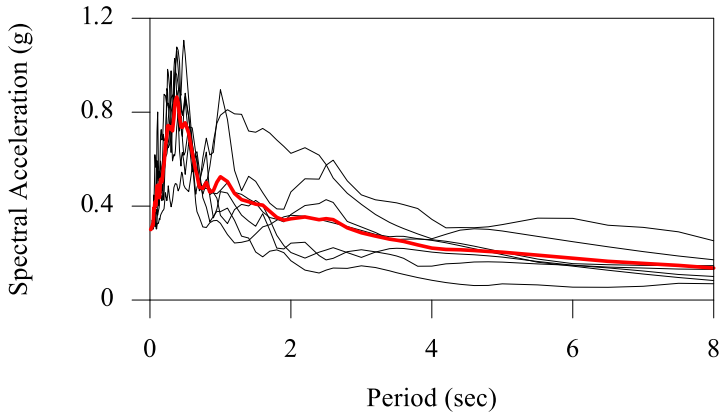

Figure 5. Response spectra of forward-directivity records

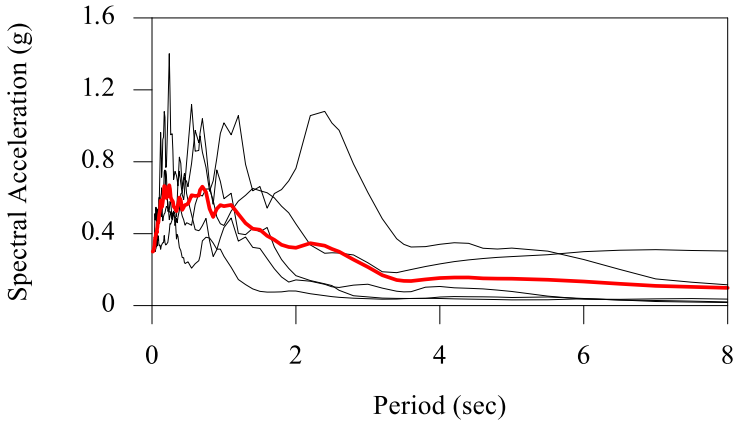

Figure 6. Response spectra of fling-step records

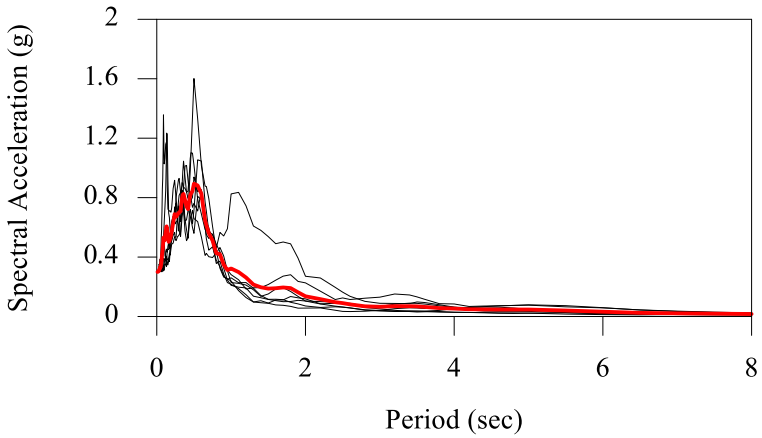

Figure 7. Response spectra of far-fault records

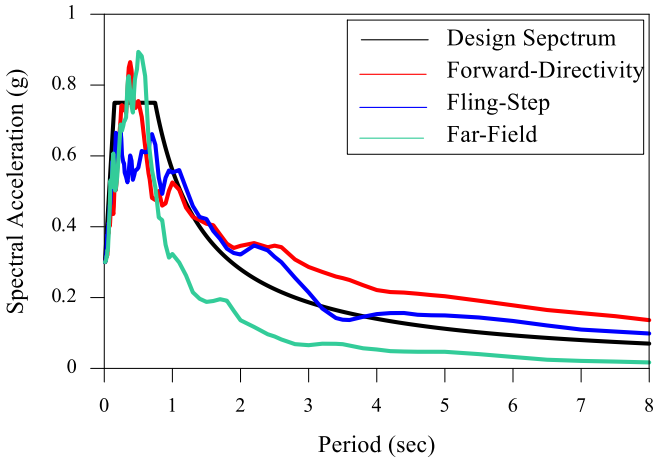

Figure 8. UBC 97 design spectrum and mean response spectra of near-fault and far-fault records

NUMERICAL CALCULATIONS

Modal Characteristics

Prior to nonlinear time history analysis of the containment structure, eigenvalue analysis of containment structure is performed to obtain its modal characteristics. Figure 9 presents the first eight vibration mode shapes and the corresponding natural periods of the containment structure. Rayleigh damping theory is a widely used damping theory in dynamic analysis of structures, and it can be described as (Chopra, 2007):

$$[C] = \alpha[M] + \beta[K] \tag{1}$$

The damping ratio for the nth mode of such a system is

$$\xi_n = \frac{\alpha}{2}\frac{1}{w_n} + \frac{\beta}{2}w_n \tag{2}$$

The coefficients α and β can be determined from the specified damping ratios ξ_i and ξ_j of the ith and jth modes, respectively. Expressing Equation (2) for these two modes in matrix form leads to

$$\frac{1}{2}\begin{bmatrix} 1/w_i & w_i \\ 1/w_j & w_j \end{bmatrix}\begin{Bmatrix} \alpha \\ \beta \end{Bmatrix} = \begin{Bmatrix} \xi_i \\ \xi_j \end{Bmatrix} \tag{3}$$

These two algebraic equations can be solved to determine the coefficients α and β. If both modes are assumed to have the same damping ratio ξ, then

$$\alpha = \xi\frac{2w_i w_j}{w_j + w_j} \quad , \quad \beta = \xi\frac{2}{w_j + w_j} \tag{4}$$

where w_i and w_j are the natural circular frequencies. In this study, the damping parameters are determined based on the dominant modes (1st and 4th) and ξ is considered as 5%. By using Equation (4), α and β parameters are determined as 1.64096 and 0.001478, respectively.

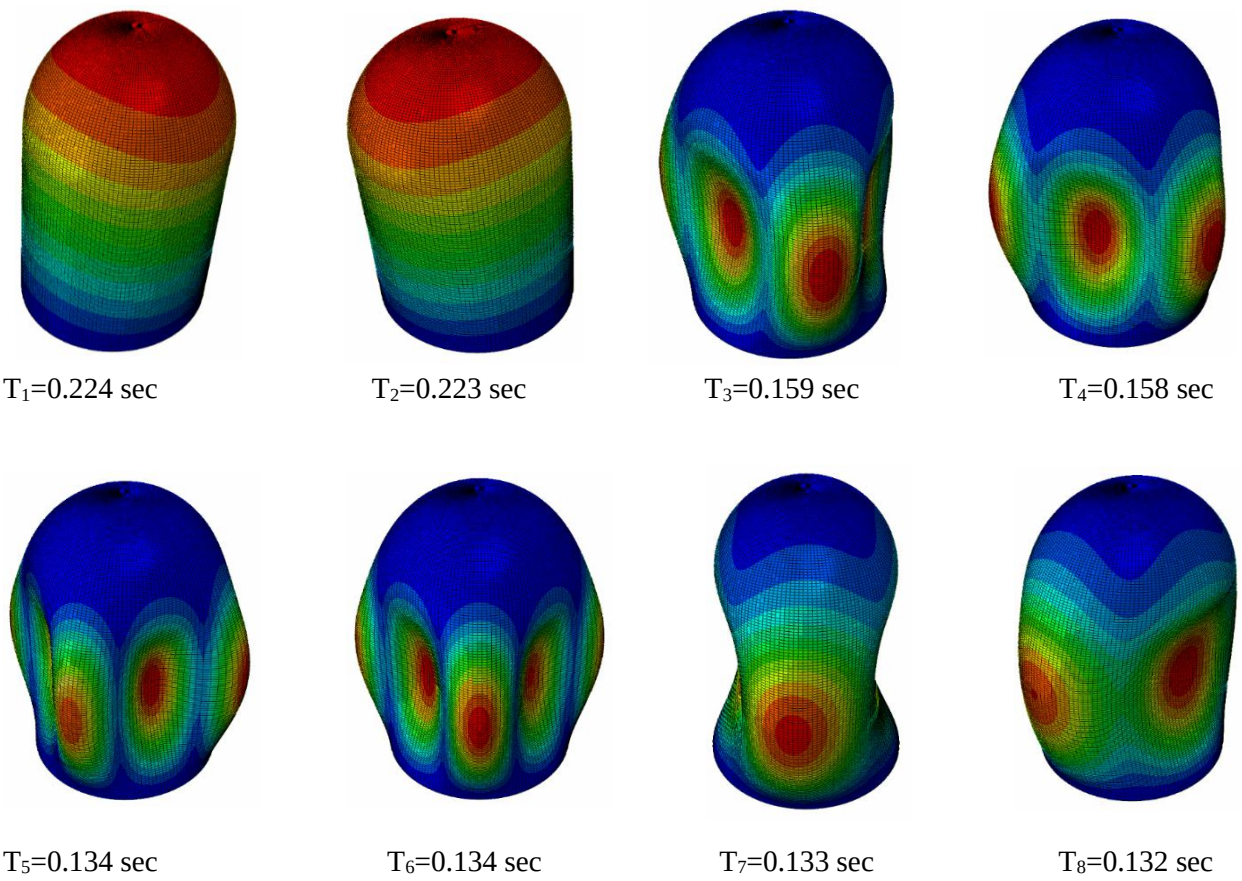

Figure 9. Mode shapes and natural periods of the containment building

Nonlinear Time-History Analysis

In this study, ABAQUS/CAE 6.11 software is used to carry out the nonlinear time-history analyses of the NPP containment building under the considered near-fault and far-fault ground motions. The near-fault ground motions showing forward-directivity and fling-step characteristics obtained from the recorded motions are applied to the NPP containment building in single horizontal direction in terms of displacement-time history records. To determine the dynamic response of the considered nuclear power plant containment building under the applied near-fault and far-fault earthquakes, structural displacements and principal stresses are compared.

Maximum horizontal relative displacements over the height of the NPP containment building are determined for each recorded ground motion component and then averaged for each ground motion group to get the mean of maximum displacements. The mean of maximum horizontal displacements obtained over the height of the NPP containment building for the considered near-fault and far-fault ground motions are compared in Figures 10-11. These displacements are the mean of maximum relative displacements over the height of the containment building with respect to the base. Because it is intended to determine the pulse type characteristics of near-fault ground motions on NPPs, first all the ground motions are normalized to have a PGA of 0.3g so that a fair comparison can be made. As an alternative normalization strategy, the ground motions are also scaled to have the same acceleration spectrum of 0.6g at the fundamental period of the NPP.

It can be noticed that the mean of maximum horizontal displacements calculated due to the forward-directivity ground motion case are the largest for both normalization cases. This can be attributed to the pulse type characteristics of near-fault ground motions showing forward-directivity characteristics. The mean of maximum horizontal displacement calculated at the top of the containment building due to the forward-directivity effect is 15.8% and 14.9% larger than the displacements calculated due to the fling-step and far-fault ground motion cases, respectively, for the normalization based on PGA (Figure 10). Mean of maximum horizontal displacements calculated for fling-step and far-fault ground motions are almost equal to each other. On the other hand, the mean of maximum horizontal displacement calculated at the top of the containment due to the forward-directivity effect is 4.8% and 11.7% larger than the displacements due to the fling-step and far-fault ground motion cases, respectively, for the normalization strategy based on the acceleration spectrum at the fundamental period of the containment building (Figure 11). It can also be observed that the mean of maximum horizontal displacements calculated for fling-step effect is larger than the far-fault ground motions. A difference of 6.6% can be noticed at the top of the containment. Based on these observations it can be underlined that due to the forward and backward motions of near-fault ground motions with forward-directivity characteristics, larger displacements are obtained.

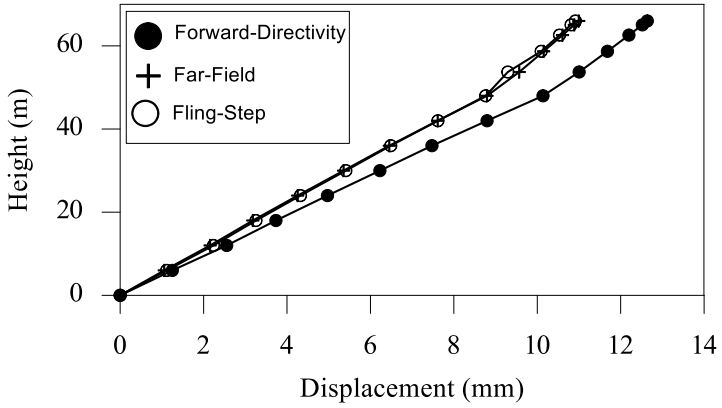

Figure 10. Mean of maximum horizontal displacements over the height of the containment building (Normalization based on PGA)

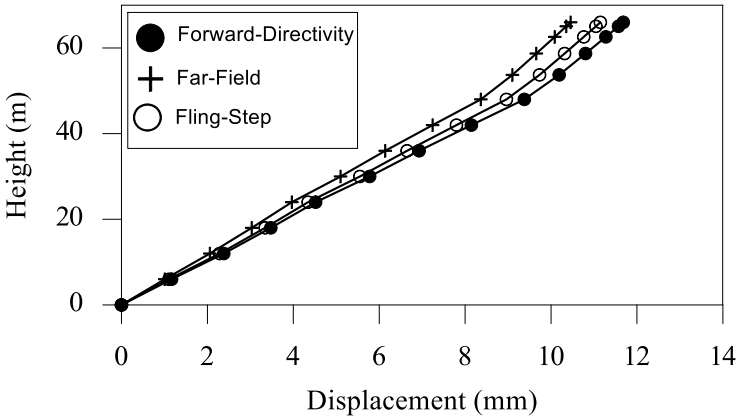

Figure 11. Mean of maximum horizontal displacements over the height of the containment building (Normalization based on acceleration spectrum at the fundamental period)

Minimum principal stresses for the considered near-fault and far-fault ground motions are compared in Table 4. The minimum principal stress obtained for each ground motion component belonging to the forward-directivity, fling-step and far-fault ground motion group are also averaged to get the mean of min principal stresses for each group of ground motions. If the mean of min principal stresses are compared, the pulse type characteristics of the forward-directivity ground motion case can also be noticed here. The mean of min principal stress due to the forward-directivity ground motion case is 8.9% and 15.9% larger than the stresses calculated due to the fling-step and far-fault ground motions, respectively, for the normalization based on PGA. Near-fault ground motion case corresponding to the fling-step effect case causes 6.4% larger stress than the far-fault ground motion. On the other hand, the mean of min principal stress due to the forward-directivity ground motion case is 8% and 16.7% larger than the stresses calculated due to the fling-step and far-fault ground motions, respectively, for the normalization strategy based on the spectrum at the fundamental period of the containment building. It can also be noticed that near-fault ground motion case corresponding to the fling-step effect causes 8% larger stress than the far-fault ground motion.

Table 4. Minimum principal stresses due to the near-fault and far-fault ground motions

	Min principal Stress (MPa)	**Mean of Min Principal Stress (MPa)**	**Min Principal Stress (MPa)**	**Mean of Min Principal Stress (MPa)**
	Normalization based on PGA		Normalization based on acceleration spectrum at the fundamental period	
Forward-Directivity				
TCU052-EW	-5.218	-6.051	-6.939	-5.534
TCU053-EW	-5.811		-5.231	
TCU068-EW	-5.955		-5.825	
TCU075-EW	-5.867		-5.118	
TCU082-EW	-5.440		-5.164	
TCU101-EW	-7.368		-4.799	
TCU103-EW	-6.695		-5.662	
Fling-Step				
TCU068-NS	-5.002	-5.554	-5.582	-5.126
TCU074-NS	-4.055		-4.298	
TCU089-NS	-11.09		-4.992	
TCU102-NS	-3.500		-6.010	
TCU129-NS	-4.125		-4.748	
Far-Fault				
CHY014-NS	-3.844	-5.220	-4.653	-4.744
CHY052-NS	-4.377		-4.801	
CHY088-NS	-4.622		-4.124	
HWA032-NS	-8.517		-4.916	
HWA034-NS	-4.801		-5.099	
HWA037-EW	-5.762		-5.010	
ILA067-EW	-4.617		-4.607	

It should also be underlined that no damage occurs in the containment building due to the considered near-fault and far-fault ground motion components. Even plastic deformations are not observed for most of the ground motions. The ground motion component of TCU089-NS normalized to the design-based earthquake intensity of 0.3g, causes the maximum structural responses. Therefore, the internal energy components of the containment building, namely the recoverable elastic strain energy, the plastic dissipation energy, and the damage dissipation energy, are plotted for this ground motion component as shown in Figure 12. It can be observed that the damage dissipation energy is zero and the contribution of the plastic dissipation energy to the internal energy is very small, indicating that the structural members of the containment building hardly reach the plastic stage.

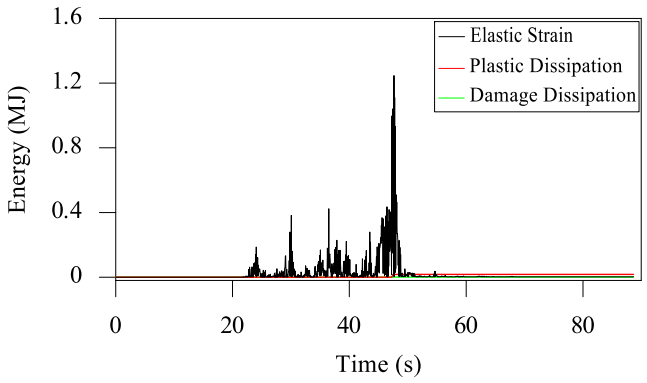

Figure 12. Internal energy components of the containment building due to the TCU089-NS ground motion

CONCLUSIONS

In this study, it is intended to perform non-linear dynamic time-history analyses of NPPs under near-fault ground motions showing directivity pulse and fling-step characteristics. The structural responses are also compared with those of the results obtained from far-fault ground motions.

Due to the forward and backward motions of near-fault ground motions showing forward-directivity characteristics, near-fault ground motions having forward-directivity effects cause around 15% larger responses than the far-fault ground motions. On the other hand, near-fault ground motions showing fling-step characteristics cause up to 8% larger responses than the far-fault ground motion case. Hence, the effect of the near-fault ground motion characteristics on the structural responses can be noticed for the selected near-fault ground motions.

Depending on the obtained results it can be concluded that especially the directivity-pulse characteristics of near fault ground motions have noticeable effects on the responses of rigid structures, like NPP containment buildings. Considering the fact that earthquakes, like Niigata Chuetsu-Oki earthquake, occur in regions very close to the nuclear power plants with ground accelerations above the design-based earthquake, near-fault effects should be considered in the design of NPP containment buildings. However, because these results are obtained just for a group of earthquake motions recorded in a single earthquake event, these results should be verified with more earthquake data.

ACKNOWLEDGEMENTS

This research is supported by the Scientific and Technological Research Council of Turkey (TÜBİTAK), as part of the International Post-Doctoral Research Fellowship Program. Project Term: 2020/1. This support is greatly acknowledged.

REFERENCES

ABAQUS 6.11. (2011). *User's Manual*, Dassault Systemes Simulia Corp., Providence, RI, USA.

Alavi, B., Krawinkler, H. (2004). "Behaviour of moment resisting frame structures subjected to near-fault ground motions". *Earthquake Eng. Struct. Dyn*, 33, 687–706.

Boore, M. (2001). "Effect of baseline correction on displacements and response spectra for several recordings of the 1999 Chi-Chi, Taiwan, Earthquake", *Bulletin of the Seism. Society of America*, 91(5), 1199-1211.

Choi, I.K., Choun, Y.S., Ahn, S.M., Seo, J.M. (2008). "Probabilistic seismic risk analysis of CANDU containment structure for near-fault earthquakes", *Nuclear Engineering and Design*, 238, 1382-1391.

Chopra, A. K. (2007). *Dynamics of Structures: Theory and Applications to Earthquake Engineering, 3rd ed.*, Prentice Hall.

Esfahani, H.M., Hejazi, F., Vaghei, R., Bin Jaafar, M.S., Karimzade, K. (2017). "Simplified Damage Plasticity Model for Concrete", *Structural Engineering International*, 1, 68-77.

EnBW-Arbeitsbericht (2008). *Besuch der japanischen Kernkraftwerke Kashiwazaki Kariwa und Tsuruga*.

Galal, K., Ghobarah, A. (2006). "Effect of near-fault earthquakes on North American nuclear design spectra", *Nuclear Engineering and Design*, 236, 1928-1935.

Darragh, B., Silva, W., and Gregor, N. (2004). "Strong motion record processing procedures for the PEER center", *Procedings of COSMOS Workshop on Strong-Motion Record Processing*, 1-12, Richmond, California, USA.

IAEA Safety Standards. (2009). *Evaluation of Seismic Safety for Existing Nuclear Installations, Safety Guide*, No. NS-G-2.13, International Atomic Energy Agency, Vienna, AUSTRIA.

International Conference of Building Officials. (1997). *Uniform Building Code*, Whittier, California.

Jin, S., Gong, J. (2020). "Damage performance based seismic capacity and fragility analysis of existing concrete containment structure subjected to near fault ground motions", *Nuclear Engng and Design*, 360, 110478.

Kalkan, E., Kunnath, S.K. (2006). "Effects of Fling Step and Forward Directivity on Seismic Response of Buildings". *Earthquake Spectra*, 22(2), 367–390.

Labbe, P., Altınyollar, A. (2011). "Conclusions of an IAEA-JRC research project on the safety significance of near-field seismic motions", *Nuclear engineering and Design*, 241, 1842-1856.

Longjun, X., Shengchao, Y., Lili, Z. (2010). "Response spectra for nuclear structures on rock sites considering the near-fault directivity effect", *Earth Eng & Eng Vib*, 9, 357-365.

Lu, X., Lin, K., Cen, S., Xu, Z., Lin, L. (2015). "Comparing different fidelity models for the impact analysis of large commercial aircrafts on a containment building", *Engineering Failure Analysis*, 57, 254-269.

Ma, Y., Ran, G., Chen, N., Lei, P., Shen, Q. (2016). "Investigation of mechanical properties and proton irradiation behaviors of SA-738-Gr. B steel used as reactor containment". *Nuclear Materials and Energy*, 8, 18-22.

Mena, J.A.A. (2016). "Earthquake soil-structure interaction modeling of nuclear power plants for near-field events", *PhD Thesis*, University of California, Davis, USA.

OriginPro, Version 2021. OriginLab Corporation, Northampton, MA, USA.

PEER Ground Motion Database, Pasific Earthquake Engineering Research Center, https://ngawest2.berkeley.edu/

Sadique, M.R., Iqbal, M.A., Bhargava, P. (2013). "Nuclear Containment Structure Subjected to Commercial and Fighter Aircraft Crash", *Nuclear Engineering and Design*, 260, 30-46.

Somerville, P.G. (2002). "Characterizing near fault ground motion for the design and evaluation of bridges", *Proc of the 3rd National Seismic Conf and Workshop on Bridges and Highways*, 137-148, Portland, USA.